Formation and Biochemical Characterization of Tube/Pelle Death Domain Complexes: Critical Regulators of Postreceptor Signaling by the *Drosophila* Toll Receptor†

David A. Schiffmann,‡ Julia H. M. White,§ Alan Cooper,|| Margaret A. Nutley,|| Stephen E. Harding,⊥ Kornelia Jumel,⊥ Roberto Solari,§ Keith P. Ray,§ and Nicholas J. Gay*,‡

Department of Biochemistry, University of Cambridge, Tennis Court Road, Cambridge CB2 1GA, U.K., Department of Molecular Sciences, Glaxo Wellcome Research and Development Ltd, Stevenage, SG1 2NY, U.K., Department of Chemistry, University of Glasgow, Glasgow G12 8QQ, Lanarkshire, Scotland, U.K., and University of Nottingham, School of Biological Sciences, NCMH Unit, Sutton Bonington, LE12 5RD, Leics, U.K.

Received February 23, 1999; Revised Manuscript Received June 21, 1999

ABSTRACT: In *Drosophila*, the Toll receptor signaling pathway is required for embryonic dorso-ventral patterning and at later developmental stages for innate immune responses. It is thought that dimerization of the receptor by binding of the ligand spätzle causes the formation of a postreceptor activation complex at the cytoplasmic surface of the membrane. Two components of this complex are the adaptor tube and protein kinase pelle. These proteins both have "death domains", protein interaction motifs found in a number of signaling pathways, particularly those involved in apoptotic cell death. It is thought that pelle is bound by tube during formation of the activation complexes, and that this interaction is mediated by the death domains. In this paper, we show using the yeast two-hybrid system that the wild-type tube and pelle death domains bind together. Mutant tube proteins which do not support signaling in the embryo are also unable to bind pelle in the 2-hybrid assay. We have purified proteins corresponding to the death domains of tube and pelle and show that these form corresponding heterodimeric complexes in vitro. Partial proteolysis reveals a smaller core consisting of the minimal death domain sequences. We have studied the tube/pelle interaction with the techniques of surface plasmon resonance, analytical ultracentrifugation and isothermal titration calorimetry. These measurements produce a value of K_d for the complex of about 0.5 μM.

The *Drosophila* dorso-ventral pathway acts to define the ventral side of the embryo and is genetically well-defined, with most of the components represented by loss-of-function alleles (*1*, *2*). Molecular cloning has helped to identify potential functions for most of these gene products and has provided evidence for their organization as constituents of a signal transduction pathway. Early during embryogenesis, the transmembrane receptor, Toll, is activated along the ventral side of the embryo by the putative ligand spätzle (*3*, *4*). The products of two genes, tube and pelle, act downstream of Toll to couple receptor stimulation to the release of the morphogen, dorsal, from its cytoplasmic anchoring protein, cactus (*5*, *6*). Once released, dorsal localizes to adjacent nuclei and regulates expression of ventral- and dorsal-specific genes involved in the establishment of dorso-ventral polarity (*7*). Several components of the DV patterning pathway, including Toll, tube and pelle, also function at later stages of development in an innate immune response stimulated by fungal pathogens (*8*). Recently, it has become clear that analogous signaling pathways mediate the innate immune response in mammals, for example, in response to bacterial lipospolysaccharides (*9*, *10*). The components in these pathways are homologues of those described in *Drosophila* DV patterning. These include human Toll receptors, IRAK kinases (*11*) (pelle) and MyD88, possibly a tube adaptor homologue (*12*).

In the Toll signaling pathway, the proteins tube and pelle act downstream of the receptor and are required for signal transduction from the receptor to dorsal. Tube encodes a protein which is localized to the cortical cytoplasm of the embryo (*13*, *14*) and mutational analysis has shown that regions required for biological function reside within the N-terminal 173 amino acids while the C-terminal half contains five octapeptide repeats of unknown function (*15*). Pelle encodes a protein with homology to members of the Raf/Mos family of serine/threonine protein kinases (*16*), but is most closely related to the mammalian IRAK proteins (*11*). Pelle protein kinase activity is essential for signaling, but

† The National Centre for Macromolecular Hydrodynamics and the Biological Microcalorimetry Facility are funded by the BBSRC and the EPSRC. D.A.S. was supported by a Studentship funded by the BBSRC and Glaxo-Wellcome. The work was also supported by grants from the Wellcome Trust and the Royal Society to N.G.

* To whom correspondence should be addressed. Phone: + 44 1223 333626. Fax: +44 1223 766002. E-mail: n.j.gay@bioc.cam.ac.uk.

‡ University of Cambridge.

§ Glaxo Wellcome Research and Development Ltd.

|| University of Glasgow.

⊥ University of Nottingham.

Abbreviations: AUC, analytical ultracentrifugation; ITC, isothermal titration calorimetry; N-pelle, residues 1−208 of pelle protein; N-tube, residues 1−257 of tube protein; PMSF, phenylmethanesulfonyl fluoride; DTT, dithiothreitol; PCR, polymerase chain reaction; S200-HR, sephacryl S200 high resolution; DV, dorso-ventral; IRAK, interleukin 1 receptor-associated kinase; SPR, surface plasmon resonance; RU, resonance unit; MALDI-TOF, matrix-assisted laser desorption time-of-flight mass spectrometry; HBS, Hepes-buffered saline; SV, sedimentation velocity; SE, sedimentation equilibrium.

10.1021/bi9904252 CCC: $18.00
Published on Web 08/19/1999

the target of pelle-dependent phosphorylation in the regulation of dorsal nuclear transport remains unclear. The N-terminal sequences of both tube and pelle have homology with so-called "death" domains, sequence motifs found in a number of signaling molecules that mediate reversible protein−protein interactions (*17*). Previous studies using the yeast two-hybrid system showed that the death domains of tube and pelle could form specific complexes in vivo (*14*, *18*, *19*). The current model of postreceptor signaling by Toll proposes that the receptors are activated by ligand-induced dimerization and that this causes recruitment to the membrane of an activation complex composed of tube, pelle, Toll, and possibly also the actin-binding protein, filamin (*19*, *20*). Thus, studies of specific binding between the tube and pelle death domains will give insights into how the Toll post receptor pathway is regulated in vivo.

In this paper, we show that specific interaction between the core death domains in tube and pelle observed in vivo is recapitulated by the purified proteins in vitro. We have characterized this interaction biochemically with analytical ultracentrifugation, isothermal titration calorimetry and surface plasmon resonance (SPR) measurements.

EXPERIMENTAL PROCEDURES

Construction of Two-Hybrid Vectors. The two-hybrid fusions between GAL4 and the appropriate domains of Toll and pelle were made using the polymerase chain reaction (PCR). Primers were designed to include restriction sites for fusion to either GAL4-BD or GAL4-AD in the two-hybrid vectors pASCYH2 and pACT2 (*21*) and were synthesized on an ABI 394 DNA/RNA synthesizer. PCR was carried out using a Perkin-Elmer 9600 PCR machine with Perkin-Elmer reagents. Pelle was generated by PCR using 500 ng of linearized plasmid S349 (*16*) as template. The DNA was treated with an initial 99 °C incubation for 10 min for denaturation and was then added to a PCR mix, comprising of 10 mM Tris-HCl, pH 8.0, 50 mM KCl, and 1.5 mM $MgCl_2$; 80 pmol of each oligonucleotide; 200 μM dNTPs and 2.5 units of *Taq*I polymerase. The reaction mix was thermally cycled 10 times at 94 °C for 30 s; 60 °C for 30 s and 72 °C for 1 min, followed by a 72 °C incubation for 10 min. The complete open reading frame of pelle (1−501) or the regulatory domain (pelle 1−208; N-pelle) was generated using a primer 5′-GCCATGGAGTCGACGATGAGTGGCGTCCAGACCGCCGAAG-3′ to the 5′-end of pelle and primers either to the putative N-terminal regulatory domain 5′-CCAGCCCCCGGGCTAGTTTTCTAGCTCCGCATAATCGATC-3′ or to full-length pelle 5′-CATAATAAGCCCGGGCTAGTCGGTAACAAACGGTTCGAAACGC-3′.

PCR products were gel purified in 0.8% low melting point agarose and fragments of the predicted size were excised and subcloned into vector pCR1000, using TA cloning reagents (InVitrogen) according to the manufacturer's instructions. The PCR clones were confirmed as being the appropriate domains of pelle and were shown as error free on both strands by dye terminator sequencing upon an ABI 373A automatic sequencer using T3, T7, and custom synthesized primers. Once verified, the pelle PCR clones were subcloned into the two hybrid vectors. All junctions were confirmed to be in frame with GAL4-BD or GAL4-AD by sequence analysis, using GAL4 primers 5′-GACAGCATAGAATAAGTGCG-3′ (GAL4-BD) and 5′-ATGGATGATGTATATAACTATCTATTCG-3′ (GAL4-AD).

Full-length tube (1−462) was cloned directly from plasmid pNB448 (*13*) as a 1.47 kb *Nco*I−*Pvu*II fragment in frame with GAL4-BD and GAL4-AD in the two-hybrid vectors pAS.CYH2 and pACT2 and confirmed by sequence analysis. The N-terminus (1−257) and the C-terminus of tube (258−462) were likewise cloned as *Nco*I−*Sal*I and *Sal*I−*Pvu*II fragments, respectively, into the two hybrid vectors. The tub2 and tub3 alleles of tube were subcloned as N-terminal (1−257 amino acid) fragments, using the *Nco*I−*Sal*I fragment as before. All GAL4 fusion junctions were confirmed by sequence analysis.

Yeast Two-Hybrid System. One microgram of purified DNA of either or both the GAL4-BD or the GAL4-AD fusion constructs in vectors pAS.CYH2 or pACT2 were transformed into yeast Y190, according to the procedure of Geitz et al. (*22*). Appropriate dilutions of cells were plated onto SD selective media, lacking either tryptophan (pAS-.CYH2-based constructs) or leucine (pACT2-based constructs) or lacking both supplements for double transformations. The yeast were incubated at 30 °C for 3−5 days before analysis of the transformants. Transactivation ability of the two-hybrid constructs was assessed by transcription of either the integrated LacZ (see below) or HIS3 reporter gene constructs within Y190. Transactivation of the HIS3 gene was assessed by the growth of transformants on SD media lacking histidine in the presence of 25 mM 3-amino-triazole, a competitive inhibitor of the HIS3 gene product.

β-Galactosidase Freeze-Fracture Assays. Transactivation of the LacZ reporter gene was determined by a freeze-fracture assay based upon the method of Breeden and Nasmyth (*23*). Yeast transformants were replica plated onto Whatman filter paper no. 54, and the replicas containing the cells were submerged twice into liquid nitrogen, allowing the filters to thaw between freezings to fracture the cells. The filters were next soaked in 2 mL of Z-buffer (60 mM $Na_2HPO_4{\cdot}7H_2O$; 40 mM $NaH_2PO_4{\cdot}H_2O$; 10 mM KCl, 0.1 mM $MgSO_4.7H_2O$; 50 mM mercaptoethanol; pH 7.0), containing 1 mg/mL of the chromogenic substrate 5-bromo-4-chloro-3-indolyl -D-galactoside (X-gal), from a freshly prepared 100 mg/mL stock dissolved in N-dimethyl formamide. Assays were developed at room temperature over a few minutes to hours.

β-Galactosidase Enzyme Assays. Crude yeast extracts for quantification of β-galactosidase activity were prepared from cells, grown to mid-logarithmic phase. One milliliter of cells was harvested, resuspended in 200 μL of Lysis buffer (0.1 M Tris-HCl, pH 7.5; 0.05% Triton X-100) and fractured using a freeze−thaw regime, whereby the cell pellet was twice alternately frozen in liquid nitrogen and thawed at 37 °C. An appropriate volume of the cell lysate was thoroughly resuspended in Z-buffer, containing 0.66 mg/mL ONPG (*o*-nitrophenyl β-D-galactopyranoside) and 50 mM β-mercaptoethanol, and the mixture incubated at 37 °C until an appropriate color developed. The reaction was stopped by the addition of 0.25 mL of 1 M Na_2CO_3, and the time of incubation was noted. Cell debris was removed by centrifugation and the optical density of the supernatant determined at 420 nm. These assays were normalized to cell numbers by resuspending 20 μL of the cell slurry to 1 mL of water and measuring the optical density at 600 nm. β-Galactosidase

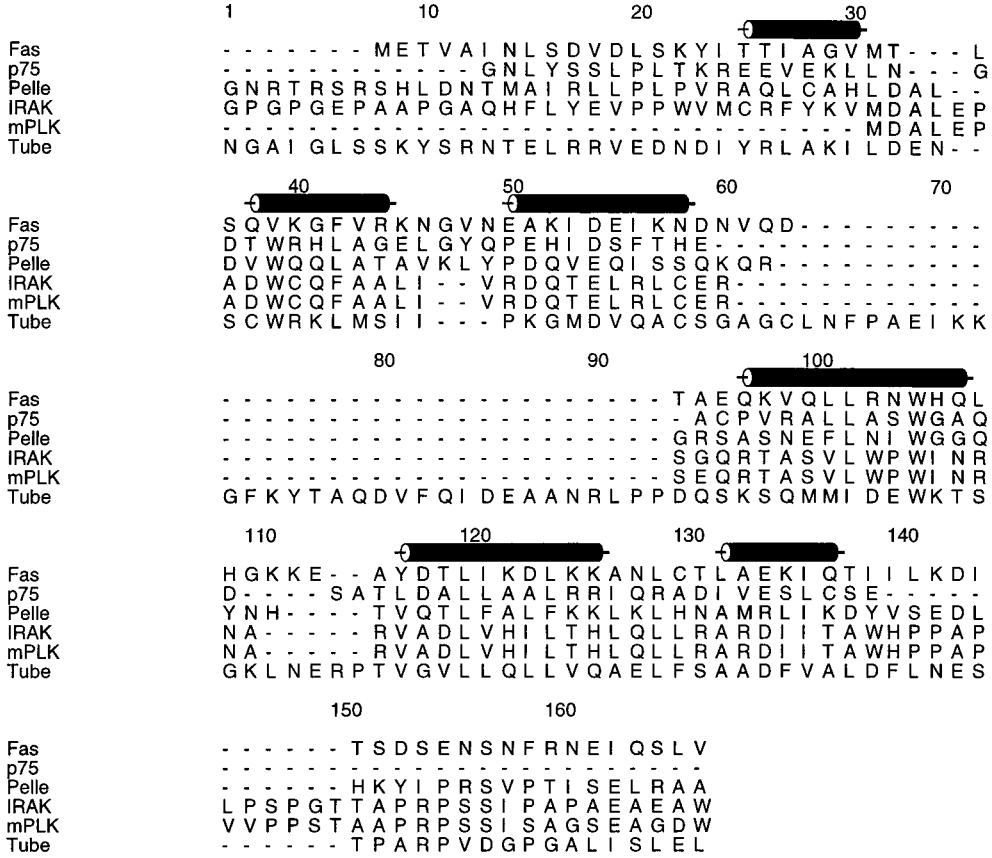

FIGURE 1: Alignment of pelle and tube with death domains of known structure. Alignments of residues within the N-terminal interaction domains of pelle and tube with proteins containing death domains of known structure. Fas (*37*); p75 (*38*); IRAK (*11*); mouse pelle-like kinase (mPLK) (*50*). The alignment was generated with JOY (*51*) and CLUSTALW (*52*) and formatted with ALSCRIPT (*53*); the positions of the α-helical segments of the death domains are indicated by the solid black cylinders. The positions of two point mutations in tube (tub2 E140K and tub3 V129D) which result in the loss of biological function and pelle interaction are located at 127 and 116 respectively in this alignment. The protease-resistant core of pelle (see Figure 4) corresponds to positions 24−140 and 26−140.

units were calculated as $U = 1000 \times A420/[A600/20]VT$, whereby V equals the volume of cell slurry added to the assay and T is the length of time of the assay.

Expression and Purification of the Tube and Pelle Death Domains. Residues 1−257 of the tube (N-tube) and 1−208 of pelle (N-pelle) were expressed using the T7 polymerase system (*24*). Primers of the following sequence were used in PCR reactions with the tube or pelle cDNA as a template. For tube: forward, 5′GCCAGGGAATTCCATATGGCGTATGGCTGGAACGGA3′; reverse, 5′GCCAGGGAATTCCATATGTTACGAGTAGTTCCGGTG3′. For pelle: forward, 5′GCCAGGGAATTCATATGAGTGGCGTCCAGACCGCCGA3′; reverse, 5′GCCAGGGAATTCCATATGTTAGTTTTCTAGCTCCGC3′. The PCR products were digested with *Nde*I and then purified after electrophoresis through low gelling temperature agarose (1%). The products were then ligated with pET3c and pET16b (Novagen) vector cut with *Nde*I and ligation mixture was transformed into *Escherichia coli* DH1. Orientation of recombinants was determined by digestion with *Pst*I (N-tube) and *Pvu*II (N-pelle). A pET3 derivative recombinant for tube (pT3/3) and pET3 and pET16 recombinants for pelle (pP3/30; pP16/34) were transformed into the T7 polymerase strain, HMS174-(DE3) (plysS).

pT3/3 directs the expression of N-tube protein to high levels, and greater than 90% of the protein forms into inclusion bodies. Cells were induced at OD_{590} 0.45 by the addition of 0.8 mM IPTG and grown for 3 h at 37 °C. The cells were collected by centrifugation, resuspended in 20 mM Tris, pH 8, 0.5 M NaCl, 1 mM DTT, 0.1% NP40, 0.1 mM EDTA, 1 mM PMSF, and 1 mM benzamidine (7.5 mL/L) and broken in the French Press at 15 000 psi. The insoluble fraction was separated by centrifugation (120000*g*, 2 h). The inclusion body pellet was washed in 10 mM Tris, pH 8, 1 mM EDTA, 0.1% NP40, and 0.5 mM PMSF and reisolated by centrifugation (10000*g*, 10 min) (three cycles). Washed inclusion bodies were dissolved in 8 M urea, 20 mM NaCl, 5 mM DTT, 0.1 mM EDTA, and 20 mM Hepes, pH 7.2, and applied to a column of SP Sepharose Fast Flow equilibrated in the same solution but with 6 M urea and 1 mM DTT. Under these conditions, nucleic acids and a 25 kDa degradation product of N-tube flow through the column with pure protein displaying retarded starting state elution. The N-tube protein is then refolded by dilution into a solution of 20 mM Hepes, pH 7.2, 50 mM NaCl, 1 mM DTT, 0.1 mM EDTA, 5% glycerol, 1 mM benzamidine, and 0.25 mM PMSF (final concentration 0.15 mg mL^{-1}). The refolding mixture is then concentrated in an Amicon-stirred ultrafiltration cell (YM10 membrane), and insoluble protein removed by centrifugation (14000*g*, 10 min). Under these conditions, more than 90% of the protein remains soluble and the preparation is more than 95% pure. The N-tube protein can be purified further by gel filtration in Sephacryl S200 HR (same buffer).

pP16/34 directs expression of histidine tagged pelle (1−208) protein (His-pelle). Cell extracts are prepared as above

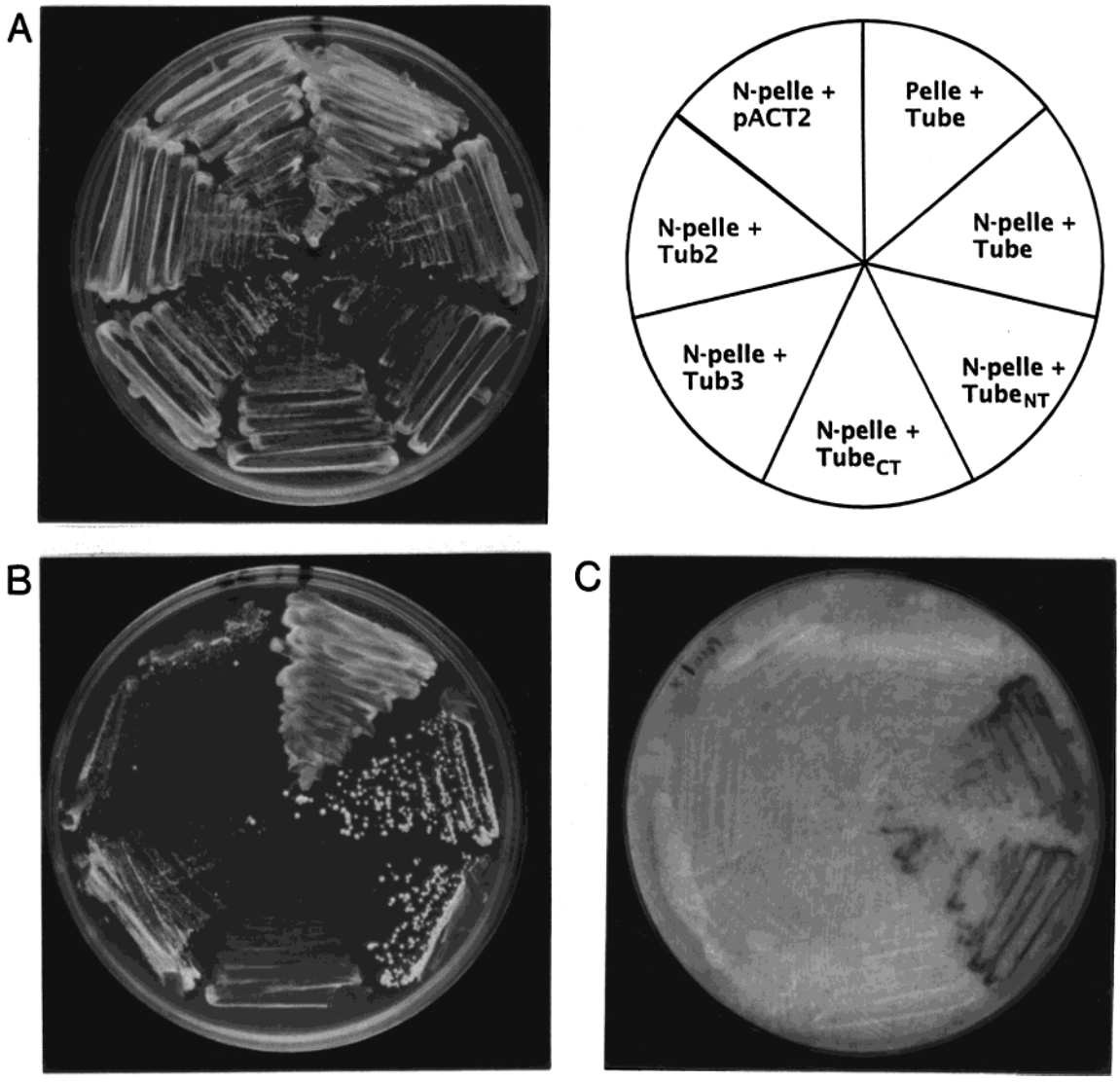

FIGURE 2: Two-hybrid interactions between pelle and tube in Y190. Domains of pelle and tube were assessed for their ability to interact in the yeast two-hybrid system by transactivation of the HIS3 and LacZ reporter genes in Y190. Transformants of the various pelle and tube constructs, as well as control vector pACT2, were plated onto SD media lacking tryptophan and leucine and grown for 3 days at 30 °C (A). Transactivation of the HIS3 reporter was determined by growth of the yeast transformants on histidine deficient SD media, in the presence of 25 mM 3-AT after five to 7 days at 30 °C (B). LacZ transactivation was assessed by blue color formation from the chromogenic substrate X-Gal, using a freeze-fracture assay on yeast grown under selective conditions (C).

except that the pellets are suspended in 20 mM Tris, pH 8, 20 mM imidazole, 0.5 M NaCl, 1 mM benzamidine, 0.75 mM PMSF, and 0.1% NP40. His-pelle is found in the soluble fraction and is purified by a column of chelating sepharose (Pharmacia) loaded with Ni^{2+}. The column is washed with 100 mM imidazole and His-pelle eluted at 500 mM. The histidine tag can be removed by treatment with Factor Xa (Biolabs). Uncleaved protein is removed by passing the digest over the Nickel affinity column and collecting the flow through (see Figure 3).

pP3/30 directs expression of untagged N-pelle 1−208 protein. Cells are grown, and extracts prepared as described above for N-tube. The soluble fraction is treated with 1 μg mL^{-1} DNase/RNase and dialyzed into a buffer containing 20 mM Bis-tris, pH 6.2, 20 mM NaCl, 5% glycerol, 1 mM DTT, and 0.1 mM EDTA (3 changes, 12−18 h). The dialysate is passed through a 0.45 μm filter and loaded on to a column of SP Sepharose Fast Flow equilibrated in the same buffer. The column is washed and eluted on a gradient of NaCl (0.02 to 0.5 M, 6 column volumes). N-pelle 1−208 elutes at ca. 0.15 M NaCl and is further purified by gel filtration in Sephacryl S200 HR, as described for N-tube.

Surface Plasmon Resonance Experiments. Surface plasmon resonance experiments were performed using a BIACORE 2000 instrument. A "CM5" biosensor chip was used to covalently bind protein (referred to as the "ligand") via amino groups to the chip. His-N-pelle was immobilized to one flowcell, using a slight modification of the manufacturer's standard protocols (*25*): after injecting the protein, 0.5% SDS was injected over the flowcell containing pelle, followed by extensive washing of the system; this was found to be necessary to obtain a useable ligand surface; ethanolamine-HCl was then injected to cap residual NHS (*N*-hydroxysuccinimide) esters on the chip matrix. BSA was immobilized by standard procedures (*25*) in another flowcell of the same chip to provide a "reference" surface. Approximately 6260 RU pelle and 5580 RU of BSA were immobilized.

Solutions of N-tube (the "analyte") diluted in "BIAcertified" HBS-EP buffer [150 mM NaCl, 3 mM EDTA, 0.005% surfactant P-20 (Tween-20), 10 mM Hepes, pH 7.4; Biacore

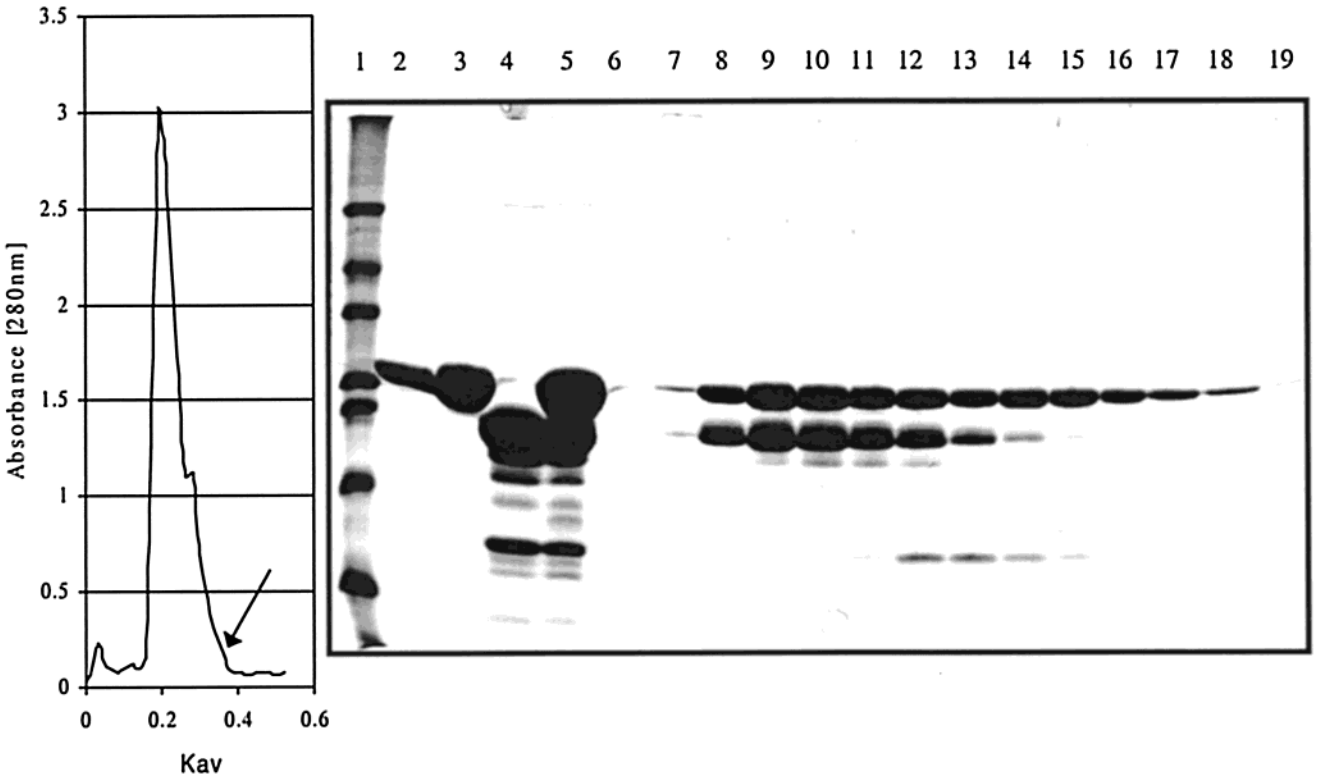

FIGURE 3: Purified tube and pelle death domains form a complex in vitro. N-tube (lanes 2 and 3) and His-pelle (1−208) were purified as described in the Experimental Procedures. His-pelle was cleaved with Factor Xa (lane 4). The proteins were mixed together (lane 5) and loaded on a column of Sephacryl S200 HR. The complexes eluted from the gel filtration column in the included volume as shown, and fractions across the major peak were analyzed by SDS−PAGE (12%) (lanes 6−19). The monomeric N-tube is separated from the complex (lanes 15 and 16). $K_{av} = (V_e - V_0)/(V_t - V_0)$, where V_e is the elution volume, V_0 is the column void volume, and V_t is the total column volume. The arrow indicates where N-tube or N-pelle run when loaded on their own.

U.K.], were injected over the chip (60 μL, 20 μL/min) in random order, in quadruplicate. Between each injection of N-tube, the surface was regenerated using 0.5 M Na_2CO_3, pH 10. The running buffer used was HBS-EP. The assays were carried out at 25 °C; data collection was set to 2 Hz, the highest rate possible for multiple flowcells. The concentrations of the N-tube and N-pelle "stock" solutions were determined by the Bradford assay using BSA as the standard.

Data were analyzed using BIAeval 3.0.2 software. After aligning the sensorgrams, the binding responses were corrected for nonspecific binding, etc., by subtracting the signal in the reference flowcell. Equilibrium analysis was performed by empirically determining the equilibrium response extrapolated to infinite time (see ref *26*), by fitting the association phase to an equation of the form:

$$R_t = (R_{eq})_1\{1 - \exp[-(k_{obs})_1 t]\} + (R_{eq})_2\{1 - \exp[-(k_{obs})_2 t]\} + X \quad (1)$$

where R_t is the response at time t and X is the sharp jump in response at the start (and end) of injection (see Supporting Information); the equilibrium response is then taken as

$$R_{eq} = (R_{eq})_1 + (R_{eq})_2 \quad (2)$$

The variation of R_{eq} with C, the concentration of injected N-tube, was fitted to the standard equation for such analysis, $R_{eq} = R_{max}K_AC/(1 + K_ACn)$ (eq 3), where n is the number of binding sites on the surface that are blocked when the analyte binds to the ligand, from which the dissociation constant, K_d, and an estimate of the maximum binding capacity of the surface, $R_{max,}$ could be determined. Based primarily on the sedimentation equilibrium experiments, n was taken to be 1.

Kinetic analysis of the data was also attempted. Data are presented here from a global fit to a heterogeneous ligand model (*27*), which assumes there are two ligand populations on the surface, each of which can bind independently to the injected component.

Analytical Ultracentrifugation (AUC) Experiments. Calculations of solvent density and viscosity, vbar estimates, 280 nm extinction coefficients, and ellipsoidal axial ratios were performed using the SEDNTERP 1.01 program (*28a*). Stock protein solutions (which contained approximately 5% glycerol for stability during freezing) were diluted into HBS buffer (150 mM NaCl, 3.4 mM EDTA, and 10 mM HEPES, pH 7.4). Sedimentation velocity (SV) experiments were performed at 4 °C on a Beckman XL-A analytical ultracentrifuge, using the absorbance at 280 nm; rotor speed was 50 000 rpm. Three samples were run: N-tube (loading concentration ~49 μM), N-pelle (~27 μM), and an approximately equimolar mixture of N-tube and N-pelle (each at ~39 μM) (concentrations based on a Bradford assay of the stock N-tube and N-pelle preparations). A total of 37 scans (for N-tube and N-pelle) or 36 scans (for N-tube/N-pelle) was fitted by nonlinear regression using the SVEDBERG program (*29*, *30*), to obtain values for the apparent sedimentation coefficient, s^*, for the three samples. The data were also analyzed by the time-derivative method to obtain the distribution of the apparent sedimentation coefficient, $g(s^*)$, based on the method of Stafford (*31*), using a

combination of his DCDT program and Microcal's ORIGIN software. *s** values from SVEDBERG were converted to conditions of 20 °C and water as buffer to give $s_{20,w}$ values, using the SEDNTERP program (*28a*). The axial ratio of the hydrodynamically equivalent prolate ellipsoid of revolution was determined using the SEDNTERP (see ftp://alpha.bbri-.org/rasmb/spin/ms_dos/sednterp) and ELLIPS1 (*28b)* programs. Sedimentation equilibrium runs were performed using Beckman XL-A and XL-I instruments. Samples of N-tube, N-pelle, and approximately equimolar mixtures of the two were loaded, and the samples were spun at 10 000, 12 000, and 15 000 rpm. The rotor temperature was 4 °C. Data suitable for analysis was obtained from cells with the following approximate loading concentrations, based on the UV_{280nm} absorbance of the stock protein solutions: N-tube (33 and 49 μM); N-pelle (17 and 27 μM); and N-tube/N-pelle approximate equimolar mixtures, where the N-tube and N-pelle concentrations were each 5, 10, 15, or 20 μM. The scans were analyzed using Beckman Origin software, the MSTARA program (*32*), and the Windows version of the NONLIN program (*33*). Using NONLIN, the scans were globally fit to a nonassociating, ideal model and to a monomer−dimer equilibrium model; the N-tube/N-pelle heteromeric interaction was approximated as a pseudo-self-association reaction, since the molecular weights of N-pelle and N-tube are relatively similar, as was done in ref *34*. Because of the low concentrations, thermodynamic nonideality was considered negligible.

Isothermal Titration Calorimetry. Isothermal titration calorimetry (ITC) experiments to measure the binding of (untagged) N-pelle to N-tube were carried out at 25.1 °C using a Microcal OMEGA titration microcalorimeter following standard instrumental procedures (*35*, *36*) with a 250 μL injection syringe and 400 rpm stirring; the tube refolding buffer was used for dilutions and buffer blank injections. Both sample and buffer blank solutions were degassed gently immediately before loading. The N-tube/N-pelle binding experiment involved 25 × 10 μL injections of N-pelle solution (180 μM) into the ITC cell (1.396 mL of active volume) containing N-tube (10.5 μM) which had been dialyzed into the same buffer. Protein concentrations in the ITC cell and syringe were determined from UV absorbance measurements at 280 nm using molar extinction coefficients, $\epsilon_{280} = 23\,950\ M^{-1}\ cm^{-1}$ for N-tube, and $\epsilon_{280} = 18\,450\ M^{-1}\ cm^{-1}$ for N-pelle, as estimated from the amino acid composition using the SEDNTERP program (*28a*). Integrated heat effects, corrected for dilution using the injection heats after complete saturation, were analyzed by nonlinear regression in terms of a simple single-site binding model using the standard Microcal ORIGIN software package. The thermal titration curve yielded estimates of the apparent number of binding sites (*N*) on the protein, the binding constant (*K*/M^{-1}), and the enthalpy of binding (ΔH/kJ mol^{-1}).

Possible homomolecular aggregation of N-tube or N-pelle was investigated using dilution ITC (*37*) involving separate injections of protein solution into buffer alone. Dissociation of oligomers in this case would give rise to a series of heat pulses (usually endothermic) from which dissociation constants and enthalpies of oligomerization may be determined.

Table 1: Assessment of β-Galactosidase Activity in Yeast Cell Extracts[a]

plasmid transfected	β-galactosidase activity (units β-Gal/unit cell density)
pASCYH2 + tube	0.61
pelle + pACT2	1.31
pelle + tube	2.26
N-pelle + pACT2	1.60
N-pelle + tube	147
N-pelle + N-tube	34.2
N-pelle + tube-CT	0.93
N-pelle + tub2-NT	0.82
N-pelle + tub3-NT	1.81

[a] Extracts were prepared from yeast Y190 cells, which had been transformed with the plasmid combinations shown. Individual transformants were selected and grown to mid-log phase as described in the Experimental Procedures. β-Galactosidase activity in the extracts was determined as described in the Experimental Procedures and the values corrected for cell density to give the activities shown (where a unit of enzyme activity is defined as ΔOD_{420nm}/min and a unit of cell density as OD_{600nm}/mL). For each transformation, cells derived from three individual transformants were combined to prepare extracts and the activities shown and are representative of three separate experiments.

RESULTS

Specific Interaction between the Tube and Pelle Death Domains Is Abolished by Mutations of Tube Which Inactivate Toll Signaling in the Embryo. It was proposed previously that the N-terminal, regulatory regions of the tube and pelle are related to death domains, reversible protein−protein interaction motifs found in a number of cytoplasmic protein involved in signal transduction (*17*). This proposal is supported by secondary structure predictions in which α-helical segments in the tube and pelle death domains align with α-helices defined in death domains of known structure (Figure 1) (*38*−*40*).

We have used the yeast two-hybrid assay to determine whether the death domains of tube and pelle can interact specifically with each other in vivo. We examined the ability of tube to associate with the pelle protein kinase (Figure 2). Expression of the full-length forms of pelle and tube provided evidence that the two proteins were able to interact weakly. Under histidine selection and in the presence of 3-AT, yeast expressing the full-length tube and pelle hybrids grew slowly due to the weak association between the proteins producing limiting quantities of the HIS3 gene product for growth. The plates were incubated for a prolonged period to enable the signal to be clearly visible (Figure 2B). The β-galactosidase signal arising from the lacZ reporter for the same two-hybrid pair was also extremely weak (Figure 2C) and was only apparent as a pale blue coloration in comparison to other stronger interactions on the same plate. Quantification of the β-galactosidase activity in extracts prepared from cells cotransfected with the tube and pelle hybrids confirmed a small but consistent increase in reporter expression relative to controls (Table 1). These results suggested that the hybrids expressed using full-length tube and full-length pelle interact weakly and confirmed previous findings.

To examine the domains of pelle and tube involved in this interaction, the putative N-terminal regulatory domain of pelle (N-pelle) was tested for its ability to interact with truncated and mutant forms of tube. Compared with full-length pelle, the N-pelle region interacted strongly with full-length tube, giving high levels of β-galactosidase (Figure

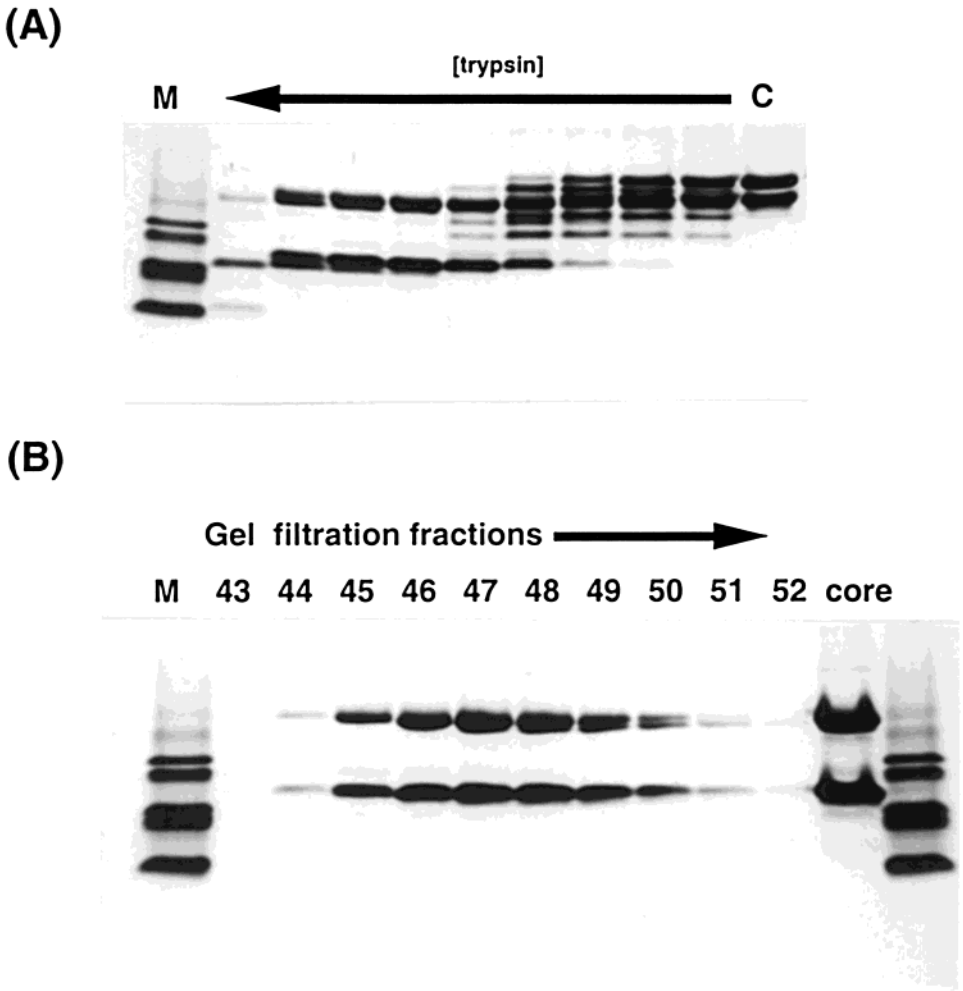

FIGURE 4: Partial proteolysis of the tube/pelle complex. (A) N-tube and N-pelle complexes were formed and purified as in Figure 3 except that N-pelle was expressed without His tag from pP3/30 and purified as described in experimental procedures. The complexes were treated with trypsin. C = untreated complex (2 mg mL^{-1}); subsequent lanes treated with trypsin for 1 h: 0.04 μg mL^{-1}; 0.08 μg mL^{-1}; 0.16 μg mL^{-1}; 0.31 μg mL^{-1}; 0.625 μg mL^{-1}; 1.25 μg mL^{-1}; 2.5 μg mL^{-1}; 5 μg mL^{-1}; 100 μg mL^{-1}; marker: 17, 14.4, 10.6, 8.2, 6.2 kDa. (B) Complex was treated with 1.25 μg mL^{-1} of trypsin for 1 h. The trypsin was then inactivated by treatment with 1 mM PMSF, the core complex concentrated to 43 mg mL^{-1} and applied to a column of S200 HR. Fractions across the single major peak of the gel filtration column were analyzed. The proteins were separated in Tris/Tricine/SDS gels (10%).

2C). These results support a model in which the tube interaction with pelle is mediated via the N-terminal domain of pelle and suggests that regions within the pelle C-terminal kinase domain may diminish the strength of this interaction, either directly or indirectly.

In further experiments, interactions between the different subdomains of tube and N-pelle were examined (see Table 1). Relative expression levels of the different tube hybrids were assessed by western immunoblotting of yeast cell extracts using a polyclonal antiserum raised against a GST-tube fusion protein. Results of two-hybrid experiments (Figure 2 and Table 1) indicated that the N-tube but not the tube C-terminal fusion protein was capable of interacting with N-pelle. On the basis of β-galactosidase production (Table 1), the level of interaction achieved between N-pelle and N-tube was much less than was measured with the full-length tube fusion. This difference may partly reflect the lower level of expression of N-tube relative to full-length tube, as judged by immunoblotting (result not shown). The N-terminal half of tube (1−257), contains a region known to be essential for dorsoventral signaling (*15*), while the C-terminal region (258−462) containing the octapeptide repeats may have a separate function. Two-hybrid experiments showed that only N-tube was capable of interacting with N-pelle.

Two embryonic lethal mutations of tube, tub2 and tub3 (Figure 1 and ref *15*), were tested for their ability to interact with N-pelle. Comparison of the tube and tub N-terminal domain fusions showed that, while the tub2 allele did not give a significant interaction with N-pelle based on growth or β-galactosidase production, the tub3 allele did show a weak though detectable response (Figure 2 and Table 1). Western blotting confirmed that both the tub2 and tub3-GAL4 AD fusions were expressed (not shown). The level of tub2 expression was similar to that seen with the wild-type N-tube; however, expression of the tub3 mutant was somewhat lower. These results suggest that the substantial loss of interaction potential of tub2 and tub 3 with N-pelle is due to the mutation.

Purified Tube and Pelle Death Domains Form Specific Complexes in Vitro. Proteins corresponding to N-pelle and N-tube, which the 2-hybrid results indicate bind together, were expressed and purified as described in the Experimental Procedures. Approximately equimolar amounts (concentration approximately 100 μM) of the proteins were mixed together for 15 min and then fractionated by gel filtration in

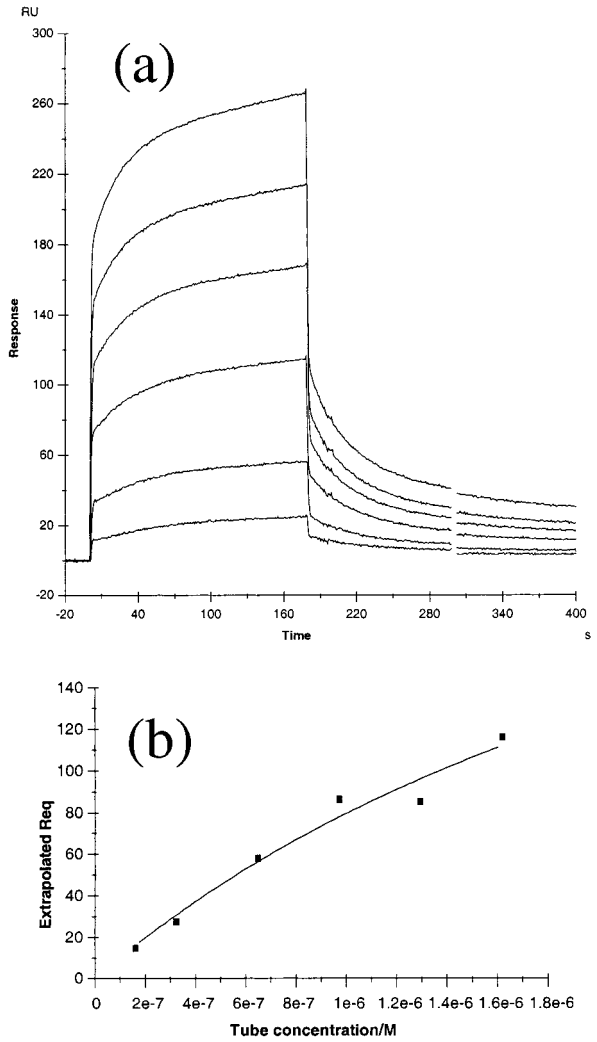

FIGURE 5: Binding of N-tube to immobilized N-pelle. (A) Sensorgrams obtained by injecting N-tube at a range of concentrations were overlaid, and the association phase of each sensorgram was fitted to a double-exponential model to obtain an estimate of the equilibrium response, R_{eq}. (B) The estimated R_{eq} values were plotted against the concentration of injected N-tube, to obtain an estimate for the equilibrium dissociation constant, K_d, by fitting to eq 3. Data shown here is from the first batch of N-tube injections. Approximate concentrations (μM) of injected N-tube were 0.16, 0.32, 0.65, 0.98, 1.30, and 1.62.

a column of Sephacryl S200 High Resolution. As shown in Figure 3, the protein complex elutes from the column in a single peak (lanes 8−12) separated from the slight excess of the N-tube monomer (lanes 15−16). This shows that the two proteins form a complex on mixing, most likely a heterodimer (see below).

A Core Death Domain Complex Is Revealed by Partial Proteolysis Experiments. Death domain complexes prepared as described above were subject to partial proteolysis with trypsin. This treatment generates a relatively stable core complex consisting of an approximately 24 kDa component and two ~13 kDa components (Figure 4A). N-Terminal protein sequencing and MALDI-TOF mass spectometry showed that the 26 kDa component is residues 2−218 of N-tube, and that the 13 kDa components consist of residues 24−140 and 26−140 of N-pelle. Proteolysis does not affect the integrity of the complex as the death domain core fractionates as a single peak in gel filtration (Figure 4B).

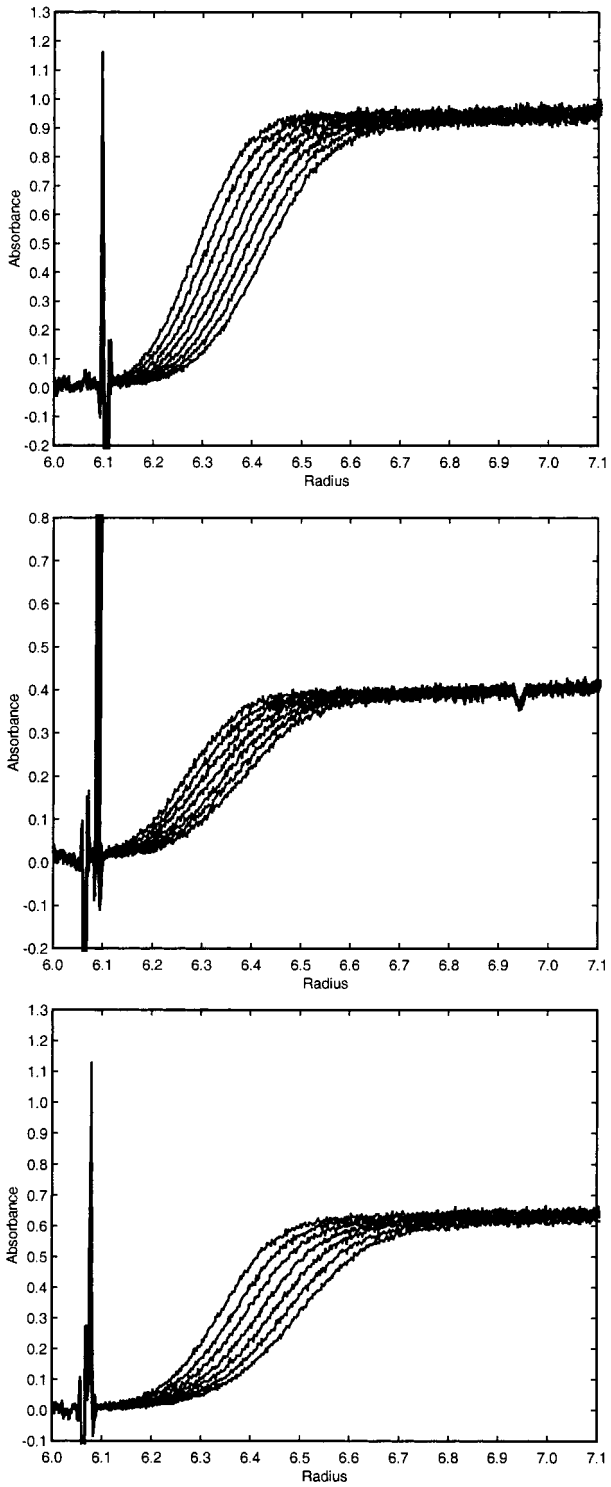

FIGURE 6: Sedimentation velocity centrifugation of N-tube and N-pelle. Absorbance scans at 280 nm of sedimentation velocity runs for N-tube (top panel), N-pelle (middle), and an approximately equimolar mixture of N-tube and N-pelle (bottom).

Analysis of the Tube/Pelle Interaction Using Surface Plasmon Resonance (Biacore) Measurements. We have studied the binding of N-tube and N-pelle using surface plasmon resonance. In these experiments, N-pelle was bound to the chip and the binding of N-tube was analyzed. Equilibrium responses for various concentrations of analyte were estimated from the sensorgrams, an example of which is shown in Figure 5a, and plotted against N-tube concentration (Figure 5b); this enabled K_d and R_{max} to be estimated

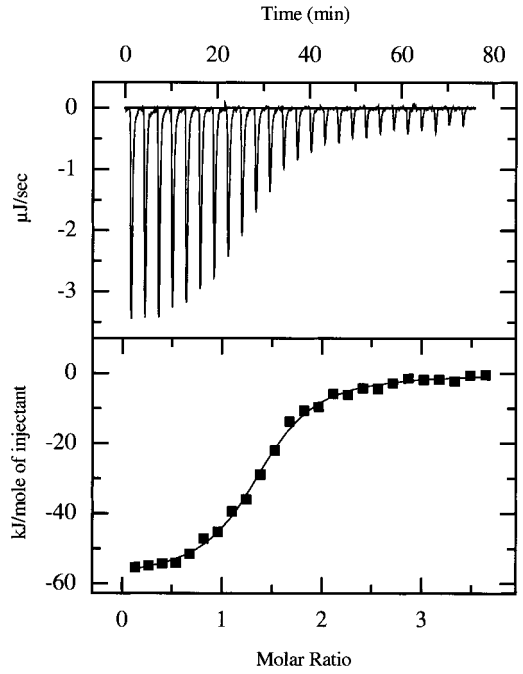

FIGURE 7: Interaction of N-tube and N-pelle measured by ITC. (A) Heat pulses generated in the microcalorimeter as a result of the individual injections of N-pelle into a sample cell containing N-tube. (B) A plot of the integrated heats for each injection, and a best-fit curve generated by nonlinear curve fitting to a simple single-site model, from which the K_d, ΔH and stoichiometry can be determined.

by nonlinear regression. This yields a mean K_d of 3.2 μM (with mean SD of 0.63 μM, $n = 4$). Kinetic analyses were also performed and this suggests that there may be two separate components in the binding, with K_d values of 1.7 and 0.8 μM (see Supporting Information).

Analytical Ultracentrifugation. N-tube and His-N-pelle death domain preparations have been studied by AUC both separately and as complexes. Representative sedimentation velocity scans are shown in Figure 6. They are smooth, sigmoidal curves, suggesting that the solutions consist of either a single, homogeneous species, multiple species with very similar sedimentation coefficients, or a rapid monomer−dimer equilibrium (*41*). Taken together with the gel filtration results and $g(s^*)$ plots, these data suggest that the solutions are monodisperse. Furthermore, the molecular weights of N-tube and N-pelle estimated on the basis of their sedimentation and diffusion coefficients, as determined from the sedimentation velocity data using either the SVEDBERG or the $g(s^*)$ analyses, are reasonably close to those expected on the basis of their known sequence and from the sedimentation equilibrium results (this is known not to be such an accurate method and very close matches are not expected); this supports the above conclusions and provides a check on the internal consistency of the analysis.

The SV scans were fitted to a one-species model using the SVEDBERG program (*29*, *30*), which gave the sedimentation coefficients, s^* and, after conversion using SEDNTERP, $s_{20,w}$ values, as shown in Table 2. Both N-tube and N-pelle have similar $s_{20,w}$ values, but the N-tube/N-pelle mixture has a significantly greater sedimentation coefficient, consistent with the formation of a heteromolecular complex upon mixing the two proteins, as seen in the gel filtration experiments reported here.

A simple analysis of the shape of the molecules in each case was performed by modeling the proteins as prolate ellipsoids; the axial ratios of such ellipsoids, which were calculated using the $s_{20,w}$ values and the mass of the protein, are shown in Table 2. The hydration ratio (w) was taken to be 0.4, which falls within the range typical for proteins and is also close to the value estimated by SEDNTERP. For such shape analysis, the N-tube/N-pelle mixture was considered as a 1:1 heteromeric complex, evidence for which comes from the sedimentation equilibrium experiments. Such analysis, which indicates a/b axial ratios significantly greater than 1, suggests that the N-tube and N-pelle death domains may have a somewhat elongated shape.

Results of globally fitting the various equilibrium scans to an ideal, monodispersed model, to obtain weight-average molecular weights, and to a monomer−dimer model to estimate the N-tube/N-pelle dissociation constant, are shown in Table 2; the density of the solvent was taken as 1.01 g/mL. For both N-tube and N-pelle, the molecular mass (M_r) obtained is close to, although slightly greater than, their calculated monomer weights. Molecular masses were also estimated by MSTARA (data not shown), which has advantages over the simpler type of analysis performed by NONLIN (*33*) in that it takes into consideration the full distribution of macromolecular solute from meniscus to cell base. These were in general consistent with those obtained from NONLIN, although they also gave M_r values somewhat higher than the monomer, which could suggest that a small amount of association is taking place, detected at the cell base and consistent with initial scans from sedimentation velocity which showed ~3−4% of fast-moving aggregate. However, there is, overall, no compelling evidence of higher-order self-association of either protein, and fitting the data as a monomer−dimer did not significantly improve the fit. A striking difference in M_r is seen, however, in cells containing the N-tube/N-pelle mixture, from both MSTARA and NONLIN analyses. Such M_r values are consistent with the formation of an N-tube/N-pelle heterodimer. The equilibrium constant for the N-tube/N-pelle association was obtained from global fitting, yielding a K_d of approximately 0.4 μM, consistent with that obtained from ITC analysis.

Isothermal Titration Calorimetry of Complex Formation by Tube and Pelle Death Domains. As a complement to the SPR and AUC studies, the interaction between N-tube and N-pelle was characterized using isothermal titration microcalorimetry (ITC), which measured the enthalpy changes that occurred when a solution of N-pelle was injected into a solution of N-tube. As for AUC, this technique has the advantage over SPR that it is a true solution technique. ITC experiments provide an independent check on the values obtained for the K_d and stoichiometry of the interaction through AUC, both these values being useful in the interpretation of the SPR studies. ITC data were consistent with exothermic single-site binding with $N = 1.25$ (± 0.05), $K_d = 0.64$ (± 0.06) μM and $\Delta H = -59.8$ (± 2.1) kJ mol^{-1}. Fitting to a two-site model, with different affinities, gave no significant improvement.

ITC was also used to look for evidence of N-tube or N-pelle self-association, by looking for heat effects upon dilution into buffer. Sequential 10 μL injections of N-tube (180 μM) or N-pelle (114 μM) into buffer, corresponding to 140-fold dilutions, gave no significant heat effects (data

Table 2: Results of Analytical Ultracentrifugation Studies on N-tube, N-pelle, and N-tube/N-pelle Complexes

physical property	N-tube	N-pelle	N-tube/N-pelle
	sedimentation velocity data		
s^* (S)[a]	1.182 (1.181, 1.182)	1.230 (1.229, 1.231)	1.703 (1.702, 1.704)
$s_{20,w}$ (S)	1.9	2.0	2.8
f/f_o	1.8	1.6	1.9
a/b ratio[b]	9.5	7.0	11.5
	sedimentation equilibrium data		
M_r (calcd) (kDa)	27.8	25.4	53.2[c]
M_r ("ideal" fit) (kDa)[a]	31.8 (30.4, 33.2)	27.6 (25.6, 29.8)	51.3 (48.7, 53.9)[d]
K_d for monomer−dimer (μM)[a]			0.37 (0.15, 0.93)[e]

[a] 95% confidence intervals for the fitted values are indicated in brackets. [b] Values shown were calculated using SEDNTERP; similar values were obtained using ELLIPS1. [c] Calculated for a 1:1 N-tube/N-pelle heterodimer. [d] Calculated using vbar for a 1:1 N-tube/N-pelle heterodimer. [e] Calculated from a global fit of the 12 useable tube/pelle equilibrium scans; the value of σ used to define the "monomer" in the NONLIN fit was determined using the mean mass of N-tube and N-pelle, and the mean vbar for these two monomers.

not shown). Consequently, there is no evidence for oligomer association over this concentration range with either protein.

DISCUSSION

In this paper, we present the first detailed biochemical analysis of death domain interactions. We have shown that two point mutations in tube (tub2, tub3), which inactivate the Toll signaling pathway in the embryo, substantially decrease the binding of N-tube to the regulatory region of pelle kinase. This indicates that physical association of tube and pelle in response to receptor activation is likely an essential step in signal transduction by Toll receptor. Alignment of the tube and pelle death domains with those of known structure suggests that the tub2 and 3 mutations lie in the region of the fifth α-helical segment and cause a charge reversal (E140K) and substitution of a hydrophobic for a charged amino acid (V129D). This suggests that the binding of the death domains might involve both hydrophobic and electrostatic interactions. However, it should be noted that the tube death domain is quite atypical, with an insert of 35 amino acids between the third and fourth helical segments (see Figure 1). Thus, tube may adopt a somewhat different overall fold to that of known death domain structures.

In light of the two hybrid data, we have expressed proteins including the death domains of tube and pelle. These proteins are monomeric in solution but when mixed together form heterodimeric complexes, consistent with the interactions observed in the 2-hybrid experiments. Partial proteolysis of this material reveals a stable, core death domain complex, a result which confirmed that these sequences mediate specific binding between the two molecules.

Analysis of complex formation by SPR gives a K_d for the interaction larger than that obtained from the ultracentrifugation and microcalorimetry experiments. This is perhaps to be expected, since the covalent immobilization of N-pelle could have impaired its ability to bind to tube; a weaker binding in such SPR experiments, compared with solution techniques, is often observed (see, e.g. refs *26* and *42*). It may also reflect the fact that, as a result of the immobilization procedure, there may be multiple populations of N-pelle on the chip surface, each with a different ability to bind N-tube, and so the K_d obtained may be a weighted average of these. In this regard, it may be significant that kinetic analysis produces a second affinity much closer to those of the other two techniques.

The sedimentation velocity results are consistent with the gel filtration data in showing the N-tube and N-pelle preparations to be monodispersed. These experiments also show that N-tube and N-pelle, if modeled as prolate ellipsoids, have axial ratios (a/b for an equivalent prolate ellipsoid) significantly greater than 1, suggesting the molecules may be asymmetric. The predicted axial ratio for the N-tube/N-pelle mixture is not significantly greater than that for either N-tube or N-pelle, which suggests the proteins may associate in a side-to-side fashion, rather than end-to-end. However, it should be borne in mind that the relatively high a/b values could also be due to large flexible loops or disordered N- or C-termini, as is suggested may be the case for the protein MKd5-AGRP (*43*). Indeed, evidence that there may be a significant disordered region in N-tube, and perhaps more so in N-pelle, comes from the partial proteolysis studies, in which a large part of each protein is cleaved off, perhaps because it is rather disordered. Analysis of sedimentation equilibrium scans yields molecular weights consistent with the formation of an N-tube/N-pelle 1:1 heterodimer; further analysis in terms of a monomer−dimer equilibrium yields a K_d for this interaction which is similar to that obtained from ITC (although the ITC-determined K_d is more reliable; see Supporting Information) and, as may be expected, is apparently somewhat tighter than the association as measured in the SPR assay. N-tube or N-pelle homodimerization, if it occurs, will be weak, but it may nevertheless be physiologically relevant, since concentrations at the plasma membrane, where these proteins are believed to localize, at least temporarily, to transduce the Toll signal (see, e.g., refs *44*), may be high enough to favor dimerization. Indeed, recent work (*45a*) suggests that such a mechanism may play a role in certain signal transduction pathways, and recent results suggest that oligomerization of tube and of pelle may be important in Toll-mediated signaling (*45b)*; control of Toll signaling through the dimerization of pelle was also suggested in ref *45c*. However, yeast two-hybrid experiments have failed to detect any pelle self-association (*19*), although, perhaps under the conditions used in this assay, the phosphorylation state of pelle was such that it precluded self-interaction [much as autophosphorylation of pelle abolishes its interaction with Toll and Tube (*45c*)]; tube self-association has not been studied in such experiments − such study is difficult because tube itself acts as a transcriptional activator in yeast (*14*, *19*; J.H.W., unpublished results).

The ITC results are consistent with those from AUC experiments; both are consistent with 1:1 complexation of N-tube and N-pelle under these experimental conditions, when uncertainties regarding protein activity are taken into account. ITC data are usually the more reliable indicators of binding stoichiometry, provided accurate concentration estimates are available, but these cannot take account of the possible effects of inactive or misfolded protein impurities. The latter seem unlikely in this case since gel filtration experiments on similar preparations gave no indication of "incompetent monomers". More likely this reflects the inherent uncertainties attached to computed molar extinction coefficients (*46*, *47*).

The results reported here suggest that the interactions mediated by death domains are relatively weak but very similar to affinities determined by similar techniques for other motifs involved in postreceptor signaling, for example SH2 domains (*48*). This finding is consistent with their function in reversible protein−protein interaction and the formation of postreceptor ternary complexes. At present there are no structures of death domain complexes, but mutagenesis studies with the TRADD domain in particular (*49*) suggest widespread sites, mainly confined to inter helix loops, contribute to homo- and heterotypic binding. One of these regions is the loop between helices 5 and 6 and it may be significant that the inactivating mutation V129K in tube may lie in the corresponding region of the tube death domain.

The biochemical analyses presented here suggest that the N-tube/N-pelle core complexes should be amenable to structural studies either by X-ray crystallography or NMR techniques. Such studies will allow the exact nature of death domain interaction to be determined and would provide further insights into how these are regulated in the context of Toll receptor activation.

ACKNOWLEDGMENT

The Biacore experiments presented here built upon earlier work by Dr. Iain Uings (GlaxoWellcome, U.K.). We thank Dr. Iain Uings and Dr. Matt Cooper (University of Cambridge) for their extensive advice and help with the BIACORE experiments and Drs. Neil Errington (University of Nottingham), Matt Deacon (University of Cambridge), and Borries Demeles (University of San Antonio) for their advice on the analysis of the AUC data. We thank Kenji Mizuguchi for preparing the death alignment, and the Protein & Nucleic Acid Facility, Department of Biochemistry, University of Cambridge, for performing the N-terminal sequencing and MALDI-MS.

SUPPORTING INFORMATION AVAILABLE

Further SPR data and discussion and further AUC data and analysis. This materal is available free of charge via the Internet at http://pubs.acs.org.

REFERENCES

1. Govind, S., and Steward, R. (1991) *Trends. Genet. 7*, 119−125.
2. St. Johnston, D., and Nusslein-Volhard, C. (1992) *Cell 68*, 201−219.
3. Morisato, D., and Anderson, K. V. (1994) *Cell 76*, 677−688.
4. Mizuguchi, K., Parker, J. S., Blundell, T. L., and Gay, N. J. (1998) *Trends Biochem. Sci. 23*, 239−242.
5. Kidd, S. (1992) *Cell 71*, 623−635.
6. Geisler, R., Bergmann, A., Hiromi, Y., and Nusslein-Volhard, C. (1992) *Cell 71*, 613−621.
7. Ip, Y. T. (1995) *Curr. Biol. 5*, 1−3.
8. Lemaitre, B., Nicholas, E., Michaut, L., Reichardt, J.-M., and Hoffmannn, J. A. (1996) *Cell 86*, 973−983.
9. Rock, F. L., Hardiman, G., Timans, J. C., and Kastelein, R. A. (1998) *Proc. Natl. Acad. Sci. U.S.A. 95*, 588−593.
10. Yang, R. B., Mark, M. R, Gray, A, Huang, A, Xie, MH, Zhang, M, Goddard, A, Wood, W. I., Gurney, A. L., and Godowski, P. J. (1998) *Nature 395*, 284−287.
11. Cao, Z., Henzel, W. J., and Gao, X. (1996) *Science 271*, 1128−1131.
12. Wesche, H., Henzel, W. J., Shillinglaw, W., Li, S., and Cao, Z. (1997) *Immunity 7*, 837−847.
13. Letsou, A., Alexander, S., Orth, K., and Wasserman, S. A. (1991) *Proc. Natl. Acad. Sci. U.S.A. 88*, 810−814.
14. Galindo, R. L., Edwards, D. N., Gillespie, S. K. H., and Wasserman, S. A. (1995) *Development 121*, 2209−2218.
15. Letsou, A., Alexander, S., and Wasserman, S. A. (1993) *EMBO J. 12*, 3449−3458.
16. Shelton, C. A., and Wasserman, S. A. (1993) *Cell 72*, 515−525.
17. Feinstein, E., Kimchi, A., Wallach, D., Boldin, M., and Varfomeev, E. (1995) *Trends Biochem. Sci. 20*, 342−344.
18. Groβhans, J., Bergmann, A., Haffter, P., and Nusslein-Volhard, C. (1994) *Nature 372*, 563−566.
19. Edwards, D. N., Towb, P., and Wasserman, S. A. (1997) *Development 124*, 3855−3864.
20. Gay, N. J., and Kubota, K. (1995) *Biochem. Soc. Trans. 24*, 35−38.
21. Durfee, T., Becherer, K., Chen, P., Yeh, S., Yang, Y., and Kilburn. A. (1993) *Genes Dev. 7*, 555−569.
22. Geitz, D., St. Jean, A., Woods, R., and Sciestl, R. H. (1992) *Nucleic Acids Res. 20*, 1425−1433.
23. Breeden, L., and Nasmyth, K. (1985) *Cold Spring Harbor Symp. Quantum Biol. 50*, 643−650.
24. Studier, F. W., Rosenberg, A. H., Dunn, J. J., and Dubendorff, J. W. (1990) *Methods Enzymol. 185*, 60−89.
25. BIAapplications Handbook (1994), Pharmacia Biosensor AB, Uppsala, Sweden.
26. Bowles, M. R., Hall, D. R., Pond, S. M., and Winzor, D. J. (1997) *Anal. Biochem. 244*, 133−142.
27. Morton, T. A., Myska, D. G., and Chaiken, I. M. (1995) *Anal. Biochem. 227*, 176−185.
28. (a) Laue, T. M., Shah, B., Ridgeway, T. M., and Pelletier, S. L. (1992) in *Analytical Ultracentrifugation in Biochemistry and Polymer Science* (Harding, S. E., Rowe, A. J., and Horton, J., Eds.) pp 90−125, Royal Society of Chemistry, Cambridge; (b) Harding, S. E., Horton, J. C., and Colfen, H. (1997). *Eur. Biophys. J. 25*, 347−359.
29. Philo, J. (1994) in *Modern Analytical Ultracentrifugation: Acquisition and Interpretation of Data for Biological and Synthetic Polymer Systems* (Schuster, T. M., and Laue, T. M., Eds.) pp 156−170, Birkhauser, Boston.
30. Philo, J. S. (1997) *Biophys. J. 72*, 435−444.
31. Stafford, W. F. (1992) in *Analytical Ultracentrifugation in Biochemistry and Polymer Science* (Harding, S. E., Rowe, A. J., and Horton, J., Eds.) pp 359−393, Royal Society of Chemistry, Cambridge.
32. Colfen, H., and Harding, S. E. (1997) *Eur. Biophys. J. 25*, 333−346.
33. Johnson, M. L., Correia, J. J., Yphantis, D. A., and Halvorson, H. R. (1981) *Biophys. J. 36*, 575−588.
34. Lebowitz, J., Kar, S., Braswell, E., McPherson, S., and Richard, D. L. (1994) *Protein Sci. 3*, 1374−1382.
35. Wiseman, T., Williston, S., Brandts, J. F., and Lin, L.-N. (1989) *Anal. Biochem. 179*, 131−137.
36. Cooper, A., and Johnson, C. M. (1994) *Methods Mol. Biol. 22*, 137−150.
37. Cooper, A. (1997) *Methods Mol. Biol. 88*, 11−22.
38. Huang, B. H., Eberstadt, M., Olejniczak, E. T., Meadows, R. P., and Fesik, S. W. (1996) *Nature 384*, 638−641.

39. Liepinsh, E., Ilag, L. L., Otting, G., and Ibanez, C. F. (1997) *EMBO J. 16*, 4999−5005.
40. Eberstadt, M., Huang, B. H., Chen, Z. H., Meadows, R. P., Ng, S. C., Zeng, L. X., Lenardo, M. J., and Fesik, S. W. (1998) *Nature 392*, 941−945.
41. Gilbert, L. M., and Gilbert, G. A. (1973) *Methods Enzymol. 27*, 273−296.
42. Kortt, A. A., Oddie, G. W., Iliades, P., Gruen, L. C., and Hudson, P. J. (1997) *Anal. Biochem. 253*, 103−111.
43. Rosenfeld, R. D., Zeni, L., Welcher, A. A., Narhi, L. O., Hale, C, Marasco, J., Delaney, J., Gleason, T., Philo, J. S., Katta, V., Hui, J., Baumgartner, J., Graham, M., Stark, K. L., and Karbon, W. (1998) *Biochemistry 37*, 16041−16052.
44. Towb, P., Galindo, R. L., and Wasserman, S. A. (1998) *Development 125*, 2443−2450.
45. (a) Stapleton, D., Balan, I., Pawson, T., and Sicheri, F. (1999) *Nat. Struct. Biol. 6*, 44−49; (b) Grosshans, J., Schnorrer, F., and Nusslein-Volhard, C. (1999) *Mech. Dev. 81*, 127−138; (c) Shen, B. H., and Manley, J. L. (1998) *Development 125*, 4719−4728.
46. Gill, S. C., and von Hippel, P. H. (1989) *Anal. Biochem. 182*, 319−326.
47. Pace, C. N., Vajdos, F., Fee, L., Grimsley, G., and Gray, T. (1995) *Protein Sci. 4*, 2411−2423.
48. Ladbury, J. E., Lemmon, M. A., Zhou, M., Green, J., Botfield, M. C., and Schlessinger, J. (1995) *Proc. Natl. Acad. Sci. U.S.A.* 92, 3199−3203.
49. Park, A., and Baichwal, V. R. (1996) *J. Biol. Chem. 271*, 9858−9862.
50. Trofimova, M., Spenkle, A. B., Green, M., Sturgill, T. W., and Goebl, M. G. (1996) *J. Biol. Chem. 271*, 17609−17612.
51. Mizuguchi, K., Deane, C. M., Johnson, M. S., Blundell, T. L., and Overington, J. P. (1998) *Bioinformatics 14*, 617−623.
52. Higgins, D. G., Thompson, J. D., and Gibson, T. J. (1996) *Methods Enzymol. 266*, 383−402.
53. Burton, G. J. (1993) *Protein Eng. 6*, 37−40.

BI9904252